JBMR Plus, 2025, **9**, ziae151
https://doi.org/10.1093/jbmrpl/ziae151
Advance access publication: November 19, 2024
Research Article

Fracture characteristics of human cortical bone influenced by the duration of *in vitro* glycation

Mei-Chun Lin[1], Praveer Sihota[1], Sofie Dragoun Kolibová[1], Imke A.K. Fiedler[1,2], Johannes Krug[1,2], Eva M. Wölfel[1], Manuela Moritz[3], Maria Riedner[4], Benjamin Ondruschka[5], Mustafa Citak[6], Felix Klebig[6], Felix N. von Brackel[1,2], Mahan Qwamizadeh[1,2], Katharina Jähn-Rickert[1,7], Björn Busse[1,2,*]

[1]Department of Osteology and Biomechanics, University Medical Center Hamburg—Eppendorf, 22529 Hamburg, Germany
[2]Interdisciplinary Competence Center for Interface Research (ICCIR), University Medical Center Hamburg-Eppendorf, 20251 Hamburg, Germany
[3]Section/Core Facility Mass Spectrometry and Proteomics, Center for Diagnostics, University Medical Center Hamburg—Eppendorf, 20251 Hamburg, Germany
[4]Technology Platform Mass Spectrometry, Universität Hamburg, 20148 Hamburg, Germany
[5]Institute of Legal Medicine, University Medical Center Hamburg-Eppendorf, 20251 Hamburg, Germany
[6]Helios ENDO-Klinik Hamburg, 22767 Hamburg, Germany
[7]Mildred Scheel Cancer Career Center Hamburg, University Cancer Center Hamburg, University Medical Center Hamburg, 20251 Hamburg, Germany
*Corresponding author: Björn Busse, Department of Osteology and Biomechanics, University Medical Center Hamburg-Eppendorf, Lottestr. 55A, 22529 Hamburg, Germany (b.busse@uke.uni-hamburg.de).

Abstract

Advanced glycation end products (AGEs) accumulate in various tissues, including bone, due to aging and conditions like diabetes mellitus. To investigate the effects of AGEs on bone material quality and biomechanical properties, an *in vitro* study utilizing human tibial cortex, sectioned into 90 beams, and randomly assigned to three mechanical test groups was performed. Each test group included ribose ($c = 0.6$ M) treatment at 7-, 14-, and 21-d, alongside control groups ($n = 5$ per group). Fluorescent AGE (fAGE) and carboxymethyl-lysine (CML) levels were assessed through fluorometric analysis and mass spectrometry, while bone matrix composition was characterized using Fourier-transform infrared and Raman spectroscopy. Mechanical properties were determined through nanoindentation and three-point bending tests on non-notched and notched specimens. The results showed significant increases in fAGEs levels at 7-, 14-, and 21-d compared to controls (119%, 311%, 404%; $p = .008$, $p < .0001$, $p < .0001$, respectively), CML levels also rose substantially compared to controls (383%, 503%, 647%, $p < .0001$, $p < .0001$, $p < .0001$, respectively). Analysis of bone matrix composition showed greater sugars/Amide I ratio at 21-d glycation compared to controls, 7-d, and 14-d ($p = .001$, .011, .006, respectively); and higher carbonate-to-phosphate ratios in the ribose treatment group compared with controls ($p < .05$) in the interstitial bone area. Mechanical testing of notched specimens exhibited a higher yield force, pre-yield toughness, and maximum force at 14-d glycation compared to controls and to both 7-d and 21-d glycation ($p < .05$). Nanoindentation showed that the hardness was lower at 7-d glycation compared to the controls and 21-d glycation ($p < .05$). In conclusion, the study found altered mechanical properties at 7 and 14 d of glycation, which then returned to control levels at 21 d, indicating a dynamic relationship between glycation duration and mechanical characteristics that deserves further exploration.

Keywords: in vitro glycation, three-point-bending, fracture mechanics, advanced glycation end products, cortical bone

Introduction

Patients with type 2 diabetes, which represent the majority of cases, can present with an elevated risk of fracture compared with non-diabetic individuals,[1] despite presenting with normal to higher bone mineral density.[2] This makes identifying diabetic patients at increased fracture risk challenging, as fracture risk predicting tools are based on bone mineral density. Furthermore, impaired bone material quality is suggested to contribute to the increased bone fragility in type 2 diabetic patients.[3]

Bone is a hierarchically structured material with individual entities at different length scales that contribute to the overall fracture toughness of bone tissue. Amongst others, the mechanical characteristics of cortical bone are critical for maintaining its functional integrity and resisting external loads. Changes in the composition and structure of cortical bone can alter its mechanical characteristics and increase fracture susceptibility.[4–7] One suggested bone matrix change associated with diabetes mellitus is the accumulation of advanced glycation end-products (AGEs), which form through the reaction of glucose or other reducing sugars with proteins in the bone matrix.[8,9] To elucidate the interplay between AGEs and bone mechanical characteristics, prior investigations have explored the accumulation of AGEs in contexts encompassing diabetes mellitus,[10] aging,[11] and chronic kidney disease.[12] Studies on human cortical and trabecular bone tissue have

Received: August 29, 2023. **Revised:** September 29, 2024. **Accepted:** November 14, 2024

demonstrated that high AGE accumulation can be a significant factor contributing to bone mechanical integrity. These changes included reduced elasticity and strength in trabecular bone,[10] compromised plasticity and toughness in cortical bone,[11] as well as diminished collagen fibril deformability at the nanoscale in cortical bone,[13] in disease states with high AGE accumulation.

Nevertheless, other studies report negligible effects on bone mechanical characteristics by AGE accumulation[14] or even enhanced bone elasticity and strength[15] within the trabecular bone in the context of type 2 diabetes mellitus.[14,15] Those aforementioned studies were carried out on bone tissue from disease conditions incorporating the naturally occurring, uncontrolled *in vivo* glycation process, thereby impeding the discernment of AGE effects on bone tissue. *In vitro* induced glycation, on the other hand, is a controlled laboratory approach that facilitates the exploration of direct AGE effects on the mechanical attributes of cortical bone while operating within precisely controlled sugar concentrations and specific exposure periods.

Reported *in vitro* glycation studies have shown different outcomes.[16–19] In cortical bone, some studies indicated alterations in bovine bone yield stress, maximum strength, and fracture toughness evaluated through 3-point bending tests,[16,19] while other studies reported no significant differences in those parameters.[17,18] Similarly, when human bone was studied, some studies reported AGEs altered fracture toughness and elastic modulus assessed with 4-point bending and microindentation,[20] whereas others found no alterations in fracture toughness and elastic properties using 4-point bending tests,[21] 3-point bending tests,[22] and nanoindentation tests.[16,18] Examining these studies, it appears that the conflicting results are due to the absence of a standardized bone fracture mechanics testing method. Additionally, variations in incubation time and experimental procedures, such as buffers, temperature, antimicrobial agents, loading rates, and type of sugar, differ among published studies. These differences could contribute to the reported literature discrepancies and influence the AGE accumulation concentration within bone tissue.

In an effort to contribute to our understanding of diabetes-induced alterations in bone material quality, this study deems to explore the repercussions of *in vitro* glycation on human cortical bone. This investigation encompasses the analysis of specific time intervals corresponding to the accumulation of AGEs. Each designated time point underwent a comprehensive assessment, combining evaluations of tissue mineral density, microstructure, mechanical properties, and bone matrix composition. The primary objective of this study is to investigate how *in vitro*-induced non-enzymatic glycation (NEG) through ribose impacts fracture properties and overall energy absorption mechanism, as well as bone collagen and mineral composition. Understanding how AGE accumulation interacts with bone fragility may offer profound insights into the intricate interplay between bone tissue alterations and mechanical integrity.

Materials and methods

Sample preparation

The bone samples were obtained from a human male organ donor with a BMI of 26.16 kg/m^1 and an age of 47 yr who had no known metabolic disease during his lifetime (IRB approval present: WT037/15). During the autopsy, a section of the mid-diaphysis of the tibia approximately 11 cm in length was extracted, immediately wrapped in phosphate buffered saline (PBS, neutrally buffered) soaked gauze, and frozen at −20 °C. A previously published report on microscale indentation demonstrated that regional hardness differences varied in the tibia diaphysis's anterior, posterior, and lateral regions but not along the anatomical axes (proximal to distal).[23] Therefore, in our study, all beams were extracted from the same region within the midshaft of the tibia. The posterior region was selected to ensure consistency across the specimens, considering that this region has the largest smooth surface. Regional selection excluded the muscle attachment areas, as well as endocortical and periosteal surfaces. The posterior part of the tibia was sawed using a bandsaw (EXAKT Advanced Technologies GmbH) to obtain a smaller specimen for the study. Using a low-speed, high-precision saw with a diamond blade (Buehler GmbH), specimens exclusively designated for subsequent mechanical analysis were longitudinally dissected into a total of 90 beams and were meticulously crafted to adhere to dimensions of 11 mm (length, L) × 1.2 mm (depth, B) × 2.4 mm (width, W) according to ASTM E1820.[24] The 90 specimens were divided into three discrete test groups, each comprised of thirty beams: (1) 3-point bending evaluation of un-notched beams (test group not intended for calculating fracture properties), (2) 3-point bending assessment notched beams (test group intended for calculating fracture properties), and (3) nanoindentation analysis (Figure 1A). For the introduction of a worst-case flaw (notched beams), a low-speed saw with thickness of 380 μm was employed to generate an initial notch at the center axis of the beam, characterized by dimensions measuring 300 μm in length and 380 μm in width.

In vitro glycation

For each mechanical testing type, prepared bone samples were randomly attributed to ribose treatment groups with 7, 14, and 21 d of glycation incubation at 37 °C ($n = 5$ for each type of mechanical testing) with three respective control groups ($n = 5$ for each type of mechanical testing). The sample size was determined based on previous work.[11] All samples were ground and polished for further analysis. The ribose solution was prepared according to previously published protocols.[19,25,26] A concentration of 0.6 M ribose is the most commonly used concentration for the glycation of bone samples *in vitro*.[26] To prevent bacterial growth, 3 mL toluene, 3 mL chloroform, and 150 mg gentamycin were added to 300 mL Hank's buffer. The control solution was prepared identically to the glycation solution except without ribose. The control and ribose-treated bone samples were placed in their respective solution in three 50 mL polypropylene tubes and incubated for either 7, 14, or 21 d at 37 °C (Figure 1B). The pH of the solutions was monitored every 7 d and maintained at pH 7.4 using 0.1 M hydrochloric acid or 0.1 M sodium hydroxide, respectively. After treatment, the samples were washed extensively with distilled water using an ultrasound water bath to remove free sugar within their treatment group. The cortical bone samples were then carefully transferred to PBS and frozen at −20 °C until further analysis.

Micro-CT

All beams were scanned using micro-CT (microCT) (microCT 40, Scanco Medical AG) with X-ray voltage of 55 kV, current of 145 μA, isometric voxel size of 10 μm, and integration time

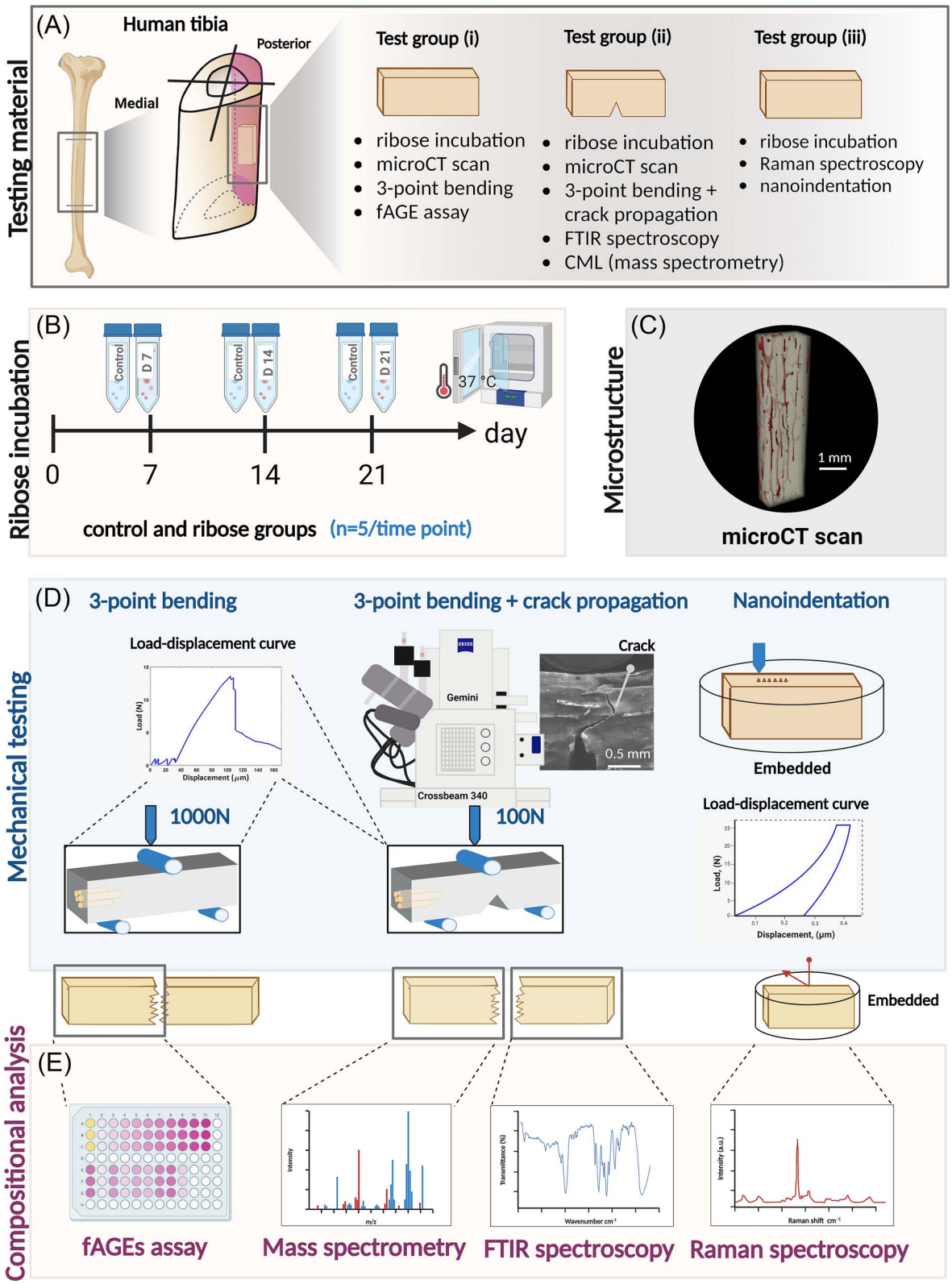

Figure 1. Study design. (A) A single tibia sample was obtained during the autopsy, with the anterior portion divided into 90 rectangular bone samples. These samples were distributed across three distinct test groups: Test group (i) for un-notched three-point bending, test group (ii) for notched three-point bending with imaging of crack propagation, and test group (iii) for Raman spectroscopy and nanoindentation. (B) Within these test groups, samples were randomly allocated to three ribose treatment durations—7, 14, and 21 d ($n = 5$ for each sample type). Corresponding control groups were incubated in ribose-free hanks buffered solution ($n = 5$ each). (C) MicroCT scanning facilitated the assessment of bone samples' microstructure, porosity, and mineralization. (D) Fracture properties of glycated bone samples were determined through micro-scale mechanical testing via nanoindentation and macro-scale testing utilizing a three-point bending apparatus for un-notched and notched bone samples. The latter involved *in situ* scanning electron microscopy imaging for crack propagation analysis. (E) Compositional analysis of the bone matrix encompassed Raman spectroscopy, quantification of total fluorescent advanced glycation end-products (fAGEs), carboxymethyl-lysine (CML), and Fourier transform infrared spectroscopy.

of 200 ms (Figure 1C). The reconstructed microCT images were analyzed using Xamflow software 1.8.11 (Lucid Concepts AG) to calculate cortical porosity (Ct.Po) and cortical tissue mineral density (Ct.TMD). The threshold for bone segmentation was set to 620 mg HA/ccm. To calculate porosity, total volume masks were created by applying a slice-wise morphological closing operation with a radial structuring element of 20 pixels (60 μm) to the binarized images, followed by filling all background voids enclosed by foreground bone pixels in 2D.

Three-point bending of un-notched bone samples

Mechanical testing of the un-notched beams was conducted using a three-point bending set-up (Figure 1D), employing a tensile-compression module (Kammrath & Weiss GmbH) equipped with a 1000 N load cell, tested in quasi-static mode with 0.05 μm/s displacement speed. The span between the two bottom supports was 10 mm. A controlled load was applied through a force applicator positioned at the opposite site between the two supports. Both the support and force applicators had a radius of 0.5 mm. Prior to testing, the samples were thawed and immersed overnight in PBS at 4 °C.

Based on the Euler–Bernoulli beam theory for 3-point bending test (See Table S2), several parameters were determined from the load–displacement curves recorded with the software provided by the manufacturer. Including maximum force (F_{max}), force at yield point (F_{yield}), stiffness, elastic modulus, work-to-fracture, and pre-yield toughness were determined using Matlab routines (Matlab R2021b, Mathworks). Specifically, F_{max} was the maximum load achieved before fracture from the load–displacement curve. The yield point was determined using a 0.2% offset method[27,28] and F_{yield} was determined as the load before yielding to plastic deformation. Stiffness was measured as the slope of the linear portion of the load–displacement curve. Elastic modulus was calculated based on the Euler–Bernoulli beam theory. The work-to-fracture (toughness, which is normalized energy) was represented as the area under the load–displacement curve divided by the cross-section (nominal fracture surface) area obtained using microCT.[29] Pre-yield toughness refers to the toughness that occurs before yielding. The beam theory formula is valid for linear elastic deformation conditions, which applies to beams with plane cross-sections that remain perpendicular to the deflection curve during linear elastic deformation. In this context, shear stress can be neglected.

Three-point bending of notched bone samples

After the ribose treatment protocols, a precise notch, measuring half the sample width ($W = 1.2$ mm), was created using a sharp razor blade and a 1 μm diamond suspension. Following the notching procedure, each specimen underwent examination under a light microscope (CX-series with CellSense software, Olympus Europa SE & Co. KG) to confirm the notch length. All samples were ground and polished using a diamond solution to smooth the surface for visualization of crack propagation.

The fracture toughness test (Figure 1D) was conducted using the previously mentioned three-point bending machine, incorporating a 100 N load cell. The sample was placed inside the vacuum chamber of a SEM (Crossbeam 340), evacuated to a pressure of 30 Pa. Subsequently, three-point bending was initiated with a pre-load of 1 N and a displacement speed of 0.05 μm/s. Crack propagation was monitored using a variable pressure secondary electron detector with an acceleration voltage of 25 kV. The magnification range was adjusted between 140× and 190×, with a working distance of 18-20 mm. Throughout the testing process, images were automatically captured at a frequency of 2 Hz and saved synchronously with force and displacement values. Finally, the loading process was terminated when the crack reached an approximate length of 1 mm.

The stress intensity factor K_I was calculated according to Fett and Munz[30,31] as follows:

$$K_I = \frac{3FL}{BW^2}\sqrt{a} * \Gamma(\alpha)$$

where B is sample thickness, W is sample width, a is crack length, α the ratio of crack length to sample thickness $\frac{a}{B}$, and the geometry factor Γ calculated as:

$$\Gamma(\alpha) = \frac{\sqrt{\pi}}{(1-\alpha)^{\frac{3}{2}}} * \left[0.3738\alpha + (1-\alpha)\sum_{\mu,\nu=0}^{4} A_{\mu\nu}\alpha^{\nu}(h/2L)^{\nu}\right]$$

Coefficients $A_{\mu\nu}$ are listed in Table 1.

Fracture toughness measurements were carried out in accordance with ASTM E1820[24] for a single-edge notched bend beam, using nonlinear elastic J-integral measurements to incorporate the role of plastic deformation in determining fracture toughness. Specifically, the J-integral [J/m^2] was computed as the sum of elastic, J_{el}, and plastic components, J_{pl}, as follows:

$$J = J_{el} + J_{pl}$$

$$J_{el} = \frac{{K_I}^2}{E}$$

$$J_{pl} = \frac{2 * A_{pl}}{B * (W - a_0)}$$

Where E is the elastic modulus calculated based on the Euler–Bernoulli beam from the un-notched beam load–displacement curve (average group value). A_{pl} is the area under the plastic region of the load–displacement curve, and a_0 is the notch length.

The crack extension was calculated using the images obtained during *in situ* SEM mechanical testing. By measuring the first crack length from the notch tip and calculating mode I crack propagation of each crack projection on the x-axis, each K_I value was obtained. K_I values against crack length (a) were plotted as crack resistance curve (R-curve), as shown in Figure 4C. Similarly, each J was calculated from the load–displacement curve, and the J against crack length (a) was plotted with a 95% confidence interval of second polynomial order by using MATLAB routines (see Figure 5A-C).

Additional parameters extracted from the load–displacement curve included maximum force (F_{max}), yield point force (F_{yield}), work-to-fracture, and pre-yield toughness, as previously described in the evaluation of un-notched beam specimens, were determined as well. However, the mechanical behavior was compared only within the same test group to ensure the validity of the results.

Table 1. Coefficients $A_{\mu\nu}$ to calculate geometry factor Γ.

	$A_{\mu 0}$	$A_{\mu 1}$	$A_{\mu 2}$	$A_{\mu 3}$	$A_{\mu 4}$
$\mu = 0$	1.1200	−0.2387	0.4317	−1.7351	2.4145
$\mu = 1$	−1.8288	−0.2573	−4.9847	16.9047	−18.2883
$\mu = 2$	2.9741	0.2706	18.6767	−60.4912	59.9239
$\mu = 3$	−2.4280	0.5627	−27.3447	87.7078	−85.2405
$\mu = 4$	0.6712	−0.5184	13.5837	−43.5421	42.3503

Raman spectroscopy

The control and glycated bone samples for Raman spectroscopy and nanoindentation were cut to 1 mm thickness along the longitudinal direction, dehydrated in an increasing series of ethanol, and infiltrated with methylmethacrylate (MMA; Merck). Samples were embedded in MMA, ground, and polished with silicon carbide paper (grit increase from P800, P1200 to P2000/4000) to a coplanar state with a microgrinder machine (EXAKT 400 CS). Each sample was analyzed with a confocal Raman spectroscope (Figure 1E) (Renishaw inVia, Renishaw plc) with a 50× objective and a laser wavelength of 785 nm. Per sample, two spectral maps of 15 array points over the polished surface were acquired, consisting of an osteonal and an interstitial region (80 μm × 20 μm), as well as 6 array points in the area of pure MMA (20 μm × 20 μm area). The exposure time was 20 s with three accumulations for each point, and the spectral range was set to 350-1750 cm^{-1}. Following spectroscopy measurements, all spectra were post-processed by subtracting a polynomial baseline using the provided software WiRE (WiRE 4.1). The polynomial order for fitting the fluorescence background was 11, with a noise tolerance 1.5 with no digital noise filtering. Automatic cosmic ray removal, spectrum normalization, and MMA spectrum subtraction were performed with the same software. Following post-processing, an average bone spectrum for each area was calculated. Subsequently, the software OriginPro 2023 (OriginLab) was used to calculate integrated areas. Following previously published methods,[32–37] two mineral-to-matrix ratios (ν_1PO_4 at 930-980 cm^{-1}/amide I band at 1620-1700 cm^{-1} and ν_2PO_4 at 410-460 cm^{-1}/amide III band at 1215-1300 cm^{-1}), crystallinity (1/full width of half maximum of ν_1PO_4), carbonate-to-phosphate ratio (ν_1CO_3 at 1050-1095 cm^{-1}/ν_1PO_4 and ν_1CO_3/ν_2PO_4), and carboxymethyl–lysine (CML)/CH_2-wag (1147-1170 cm^{-1}/1432-1490 cm^{-1}) ratio were measured.[32,36] We also calculated the amide I sub-peak ratios based on the sub-band fitting to investigate collagen helical status (I_{1670} at ∼1670 cm^{-1}/I_{1640} at ∼1640 cm^{-1}),[35,37] and collagen matrix maturity (I_{1670} ∼ 1660 cm^{-1}/I_{1690} ∼ 1690 cm^{-1}).[33,37]

Nanoindentation

Following Raman spectroscopy, specimens were further polished with 3 μm diamond suspension, followed by 1 μm diamond suspension until final polishing with 0.05 μm aluminum oxide suspension to diminish surface roughness, following previously published methods.[38] The samples were washed with ultrasound water baths in distilled water to remove surface debris.

Fine-polished specimens were indented in the longitudinal osteonal direction utilizing an iMicro nanoindenter (KLA Instruments) equipped with a Berkovich tip (Figure 1D). Per specimen, a total of 40 indentations were performed in two regions, ie, osteonal and interstitial bone region. In each region 20 indents were placed with lateral distance of 30 μm and indentation depth of 2 μm employing the depth-sensing continuous stiffness method. Young's modulus and hardness were determined based on the approach proposed by Oliver and Pharr,[39] considering a Poisson's ratio of 0.3. These calculations were performed using the InView Run Test software provided by the manufacturer (KLA Instruments). Before and after each measurement, the tip was calibrated on fused silica.

Fourier transform infrared spectroscopy

Fourier transform infrared spectroscopy (FTIR) was performed to obtain the relative sugar content of the bone matrix (Figure 1E). Notched samples after 3-point bending were cut with longitudinal direction of the beam and demineralized using a 20% EDTA solution in PBS. The bone tissue was submerged in the EDTA solution for 3 mo at room temperature, with changes of EDTA solution twice a week. After 3 mo, the demineralized tissue was rinsed twice with acetone for 10 min, then twice with distilled water for 10 min, and 70% ethanol before spectrum acquisition. The spectra were collected with a FTIR Spotlight 400 (PerkinElmer) attached to a FTIR Spectrometer Frontier (PerkinElmer). The spectra were acquired in a reflective transmittance mode over a spectral range of 2000-650 cm^{-1} at a resolution of 4 cm^{-1} with 60 accumulations per scan. The characteristic peaks of the standard were found using the spectrum software of the manufacturer. The software OriginPro 2023 (OriginLab) was used for baseline correction and to calculate peak intensities and areas under the curve. The sugar-to-matrix ratio was determined by dividing the area of the sugar peaks (νCO and νCC peaks located between 900 and 1100 cm^{-1}) by the amide I peak (1596-1712 cm^{-1}) according to previously published protocols.[15]

fAGE—fluorometric analysis

Total fluorescent AGEs (fAGEs) were quantified using fluorescence spectroscopy and normalized to collagen content assessed by colorimetric assay (Figure 1E).[26] Unfixed frozen, broken halves of the beams after the un-notched mechanical test were defatted by alternated soaking for 15 min in either 70% ethanol or saline. After 18 h of lyophilization, the bone samples were hydrolyzed in 6 M HCl (10 μL of HCl per mg of bone) at 110 °C for 16 h. Bone hydrolysates were diluted in deionized water to a final concentration of 0.5 mg bone/mL and centrifuged at 13 000 rpm at 4 °C. The collected supernatant was utilized for the remaining steps of the assay. In the fluorescence assay, the measurement was performed with the serially diluted quinine standards (stock solution 10 μg quinine per mL of 0.1 N H_2SO_4) and bone hydrolysates in a 96-well plate using the multi-mode

microplate reader at excitation of 360 nm and emission of 460 nm. All measurements were carried out in triplicates, darkness, and room temperature. The total content of collagen in the bone tissue was determined using a colorimetric assay of hydroxyproline using hydroxyproline standards (stock solution 2 mg/mL hydroxyproline in 0.001 N HCl). First, chloramine-T (0.06 M chloramine-T in a solution of deionized water, 2-metoxyethanol, and hydroxyproline buffer in 2.3:5, respectively) was added to the bone hydrolysates and standards in a 1:2 ratio following incubation in the dark at room temperature for 20 min to oxidize hydroxyproline. The reaction was stopped by adding 4.5 M perchloric acid. Finally, *p*-dimethylaminobenzaldehyde (200 mg/mL in 2-metoxyethanol) was added and the samples and standards were incubated at 60 °C for 20 min to produce a chromophore. The absorbance of bone hydrolysates and hydroxyproline standards was measured in triplicates at 570 nm in a 96-well plate using a multi-mode microplate reader (Inifinite 200, Tecan Group Ltd.). Collagen content is determined based on the assumption of bone's composition of 14% hydroxyproline.[40] The total fAGEs are presented in ng quinine fluorescence/mg collagen content.

CML—non-fluorescence analysis

Total CML was quantified using mass spectrometry (Figure 1E). N6-(carboxymethyl)-L-lysine was purchased from Cayman Chemicals (Item No. 16483). [$^2H_4$]-N6-(carboxymethyl)-L-Lysine was purchased from Alsachim. Stock solutions of both substances were prepared with LC–MS grade water at a concentration of 1 mg/mL. For the quantification of CML, different concentration levels ranging from 5 to 500 ng/mL were prepared in 0.1% formic acid (FA).

The unfixed, frozen, broken halves of the notched beams after the mechanical test were defatted by alternated soaking for 15 min in either 70% ethanol or saline. After 18 h of lyophilization, the bone samples were hydrolyzed in 6 M HCl (10 μL of HCl per mg of bone) at 110 °C for 16 h. Bone hydrolysates were diluted in deionized water to a final concentration of 0.5 mg bone/mL and centrifuged at 13 000 rpm at 4 °C.

Bone hydrolysates were dried in a vacuum centrifuge and resuspended in 200 μL water (LC–MS grade). Oasis HLB Plus LP Extraction Cartridges (Waters Corporation, PN 186000132) were used for sample clean-up prior to mass spectrometric measurements. The cartridges were conditioned with 3 mL methanol and equilibrated with 3 mL water. After sample loading, the cartridges were washed with 3 mL of 5% (v/v) methanol. CML was eluted with 2 mL methanol. The eluates were dried in a vacuum centrifuge and resuspended in 400 μL of 0.1 % (v/v) FA. An aliquot of 4 μL was injected into the liquid chromatography–tandem mass spectrometry (LC–MS) system.

LC–MS/MS measurements were performed on an Agilent 1290 Infinity II LC system coupled to an Ultivo triple quadrupole mass spectrometer (Agilent Technologies). Liquid chromatography was run on an XBridge Premier BEH Amide VanGuard FIT Column, 2.5 μm, 2.1 mm × 150 mm (Waters Corporation, PN 186009933) kept at 40 °C. The column was operated in HILIC mode, therefore equilibrated with 90% eluent B (0.1% FA in acetonitrile) and 10% eluent A (0.1% FA in water) delivered at a flow rate of 0.5 mL/min. Further details of the gradient used for the LC–MS/MS runs are given in Table S3.

N(6)-carboxymethyllysine was quantified using positive electrospray ionization (ESI) and multiple reaction monitoring (MRM) mode. The optimal precursor and product ions, fragmentor voltages, and collision energies (Table S4) were obtained and optimized by Agilent MassHunter Acquisition Optimizer software. For this, standard solutions of CML and CML-d4 were used at a concentration level of 1000 ng/mL.

The quantifier MRM transitions were selected based on the most intense fragment ion. They were m/z 205.1 → 84 and m/z 209.1 → 88.1 for *N*(6)-Carboxymethyllysine and [$^2H_4$]-N6-(carboxymethyl)-L-Lysine, respectively. Moreover, the MRM transitions used as qualifier were m/z 205.1 → 130 and m/z 205.1 → 56 for *N*(6)-Carboxymethyllysine, and m/z 209.1 → 134.3 and m/z 209.1 → 58.1 for CML-d4 (Table S5). The source parameters were set as the following: gas temperature 300 °C; gas flow 8 L/min; nebulizer gas 35 psi; capillary voltage 4000 V; sheath gas temperature 300 °C; sheath gas flow 11 L/min; and nozzle voltage 1500 V.

Data was processed with Mass Hunter Quantitative Data Analysis software (Version 10.0). The calibration levels ranged from 5 to 500 ng/mL, displaying linear responses throughout the concentration range with R^2 values greater than 0.998. The recovery rate of [$^2H_4$]-N6-(carboxymethyl)-L-Lysine was calculated, and the quantified amounts of *N*(6)-carboxymethyllysine were corrected accordingly. The corrected CML quantities were additionally normalized to the dry weight of the bone samples.

Statistical analysis

Statistical analysis was performed using Prism (9.5.1, GraphPad). Shapiro–Wilk test was used to analyze normality, and the normally distributed data was compared between groups using ANOVA tests for statistical analysis. Pearson correlation was used for analyzing linear relationships between compositional and mechanical properties. As control samples did not show differences in all parameters with regard to incubation times, all control samples were combined into one control group ($n = 15$) to compare to each glycation group ($n = 5$). Tukey multiple comparison test was used as a post hoc test at a significance level of 0.05. The outliers were defined and excluded with Grubbs' test (significance level = 0.05).

Results

Increased fAGEs and CML levels in glycated human cortical bone specimens

All specimens exhibited uniform microstructural characteristics, as evidenced by comparable measurements of Ct.TMD and Ct.Po, as detailed in Table 2 and assessed through microCT imaging. The quantification of total fAGEs and CML was conducted to ascertain the impact of *in vitro* glycation-induced non-enzymatic cross-linking. Subsequent to glycation periods spanning 7, 14, and 21 d, fAGE levels exhibited notable elevation in contrast to control instances, displaying an incremental rise over the incubation duration. Total fAGEs measured 117.11 ± 26.94 ng of quinine/mg of collagen in controls, 256.90 ± 18.21 ng of quinine/mg of collagen in the 7-d ribose treatment group, 482.46 ± 84.43 ng of quinine/mg of collagen in the 14-d ribose treatment group, 591.05 ± 99.36 ng of quinine/mg of collagen in the 21-d ribose treatment group. Specifically, specimens subjected to 7, 14, and 21-d ribose treatment displayed an average

Table 2. The microstructure of bone samples was similar in all groups (all control samples were combined into one control group ($n = 15$) to compare to each glycation group ($n = 5$)).

	Control	D7	D14	D21
Ct.Po [%]	3 ± 1	2.7 ± 0.9	3 ± 1	3 ± 0.6
Ct.TMD [mgHA/ccm]	1169.4 ± 14.8	1176.8 ± 15.7	1179.9 ± 18.4	1169.2 ± 7.6

Data are shown as mean ± SD. Data were analyzed using ANOVA with the Tukey post hoc test. Cr.Po $p = .976, .963, .387$ for control vs D7, control vs D14, and control vs D21, respectively; $p > .999, .757, .784$ for D7 vs D14, D7 vs D21, and D14 vs D21, respectively. Ct.TMP $p = .769, .536, > .999$ for control vs D7, control vs D14, and control vs D21, respectively; $p = .988, .845, .667$ for D7 vs D14, D7 vs D21, and D14 vs D21, respectively. D7, 7-d ribose treatment; D14, 14-d ribose treatment; D21, 21-d ribose-treatment; Ct.Po, cortical porosity; Ct.TMD, cortical tissue mineral density.

increase of 119%, 311%, and 404% relative to controls ($p = .008$, $p < .0001$, $p < .0001$, respectively). Moreover, 14 and 21-d ribose treatment had 88% and 130% elevated fAGEs content compared with 7-d ribose treatment ($p = .001$, $p < .0001$, respectively), as shown in Figure 2A. Similarly, the CML content measured 16.25 ± 1.24 ng/mg bone tissue in controls, 78.44 ± 11.48 ng/mg bone tissue in the 7-d ribose treatment group, 97.98 ± 14.23 ng/mg bone tissue in the 14-d ribose treatment group, 121.5 ± 7.44 ng/mg bone tissue in the 21-d ribose treatment group, showing a noticeable increase after 7, 14, and 21 d of ribose incubation compared with controls (383%, 503%, 647%, $p < .0001$, $p < .0001$, $p < .0001$, respectively). Additionally, 14- and 21-d ribose treatment led to 25%, 56% elevated CML content compared with 7-d ribose treatment ($p = .039$, $p < .0001$), and 21-d ribose treatment resulted in 24% elevated CML content compared with 14-d ribose treatment ($p = .013$), as shown in Figure 2B. To determine the effects of glycation on sugar composition, FTIR spectroscopy analysis were performed and the corresponding FTIR spectra were analyzed (Figure 2C). The sugar-to-matrix ratio exhibited a distinct elevation at 21-d ribose treatment in contrast to the controls, 7, and 14-d ribose treatment ($p = .001, .011, .006$, respectively), as shown in Figure 2D.

Elevated carbonate-to-phosphate ratios in glycated interstitial bone

Raman analysis was performed to determine the effects of glycation on the bone matrix composition. Representative spectra are shown in Figure 3A and B. The regions of different tissue ages were investigated, namely younger osteonal and older interstitial bone (Figure 3C). In the interstitial bone matrix, significant differences were observed in the carbonate to phosphate ratios: The ratio ν_1CO_3/ν_1PO_4 was higher after 7- and 21-d glycation compared to controls (Figure 3D; mean difference 4.06%, 4.59%, $p = .0203$, $p = .009$, respectively), and ν_1CO_3/ν_2PO_4 ratio was higher after 14- and 21-d glycation compared to controls (Figure 3E; mean difference 9.10%, 7.18%, $p = .008$, $p = .036$, respectively). The non-fluorescent AGE CML ratio (Figure 3F) did not differ between glycation and control groups. No differences for the above-mentioned parameters were detected in the osteonal bone matrix (Figure 3G-K). Additional Raman spectroscopy parameters are summarized in Table S1.

Altered mechanical properties in glycated bone specimens

Mechanical properties of ribose treatment and control bone samples were assessed using three different test groups: un-notched and notched 3-point bending as well as nanoindentation. Among the un-notched beams, no notable differences were discerned between the groups, showing comparable maximum and yield force alongside pre-yield toughness values determined based on work-to-fracture calculation, *E*-modulus, and post-yield displacement (Table 3). For the analysis of fracture mechanics in notched beams, visualization of crack propagation (Figure 4A) accompanied by concurrent force-displacement records (Figure 4B) and *R*-curve (Figure 4C) was performed. The yield point force (F_{yield}) showed that the 7- and 14-d ribose treatment groups had significantly higher values than the control (16.21 ± 2.38 N for the 7-d, 17.21 ± 2.10 N for the 14-d vs 12.75 ± 3.29 N for the control, $p = .0149$, $p = .001$, respectively), followed by a lower value at the 21-d ribose treatment, returning to the control level (7-, 14-d vs 11.35 ± 2.07 N for the 21-d, $p = .015$, $p = .002$; respectively), as shown in Figure 4D. The maximum force (F_{max}, Figure 4E) was higher at 14-d ribose treatment and lower at 21-d ribose treatment group (20.16 ± 2.33 N for the 14-d vs 14.66 ± 1.33 N for the 21-d, $p = .028$), but no significant difference compared to the control group. The pre-yield toughness exhibited a substantially higher value at the 7-, and 14-d ribose treatment in comparison to the control group (473.6 ± 190.8 J/m^2 for the 7-d, 522.20 ± 82.57 J/m^2 for the 14-d, vs 286.40 ± 82.57 J/m^2 for the control, $p = .049$, $p = .004$, respectively), followed by a noticeably lower value at the 21-d ribose treatment, returning to the control level (14-d vs 264.50 ± 78.33 J/m^2 for the 21-d, $p = .009$), as shown in Figure 4F. The post-yield toughness showed significantly lower at the 14-d ribose treatment group compared to the control (657.20 ± 18.70 N for the 14-d vs 970.30 ± 218.70 N for the control, $p = .03$), as shown in Figure 4G.

The slope of the *R*-curve determines the growth toughness. Due to technical issues, there were two crack image data losses in the 7-d treatment group; the rest of the data demonstrated a lower growth toughness with 7-d ribose treatment group yet no significant difference between the groups (Figure 4H). Overall fracture toughness exhibited similarity among the groups, with values of 2.38 ± 0.78 MPa$\sqrt{m}$ in control; 2.62 ± 1.14 MPa$\sqrt{m}$ at 7-d ribose treatment; 2.45 ± 0.45 MPa$\sqrt{m}$ at 14-d ribose treatment; 2.57 ± 0.38 MPa$\sqrt{m}$ at 21-d ribose treatment.

The elastic *J*-integral at yield point ($J_{el0.2\%}$) values demonstrated no significant variations between the groups. Yet, the plastic *J*-integral at yield point ($J_{pl0.2\%}$) was significantly higher in the 7-d ribose treatment group compared to the controls ($p = .046$) and followed by a decrease after the 21-d ribose treatment to control level ($p = .049$ compared with 7-d ribose treatment group) (Figure 4I).

The results of nanoindentation as a measure of nanomechanical elastic properties are shown in Table 4. Osteonal bone areas showed statistically similar elastic modulus and hardness in the control and ribose treatment groups spanning 7, 14, and 21 d ($p > .05$). The elastic modulus in the

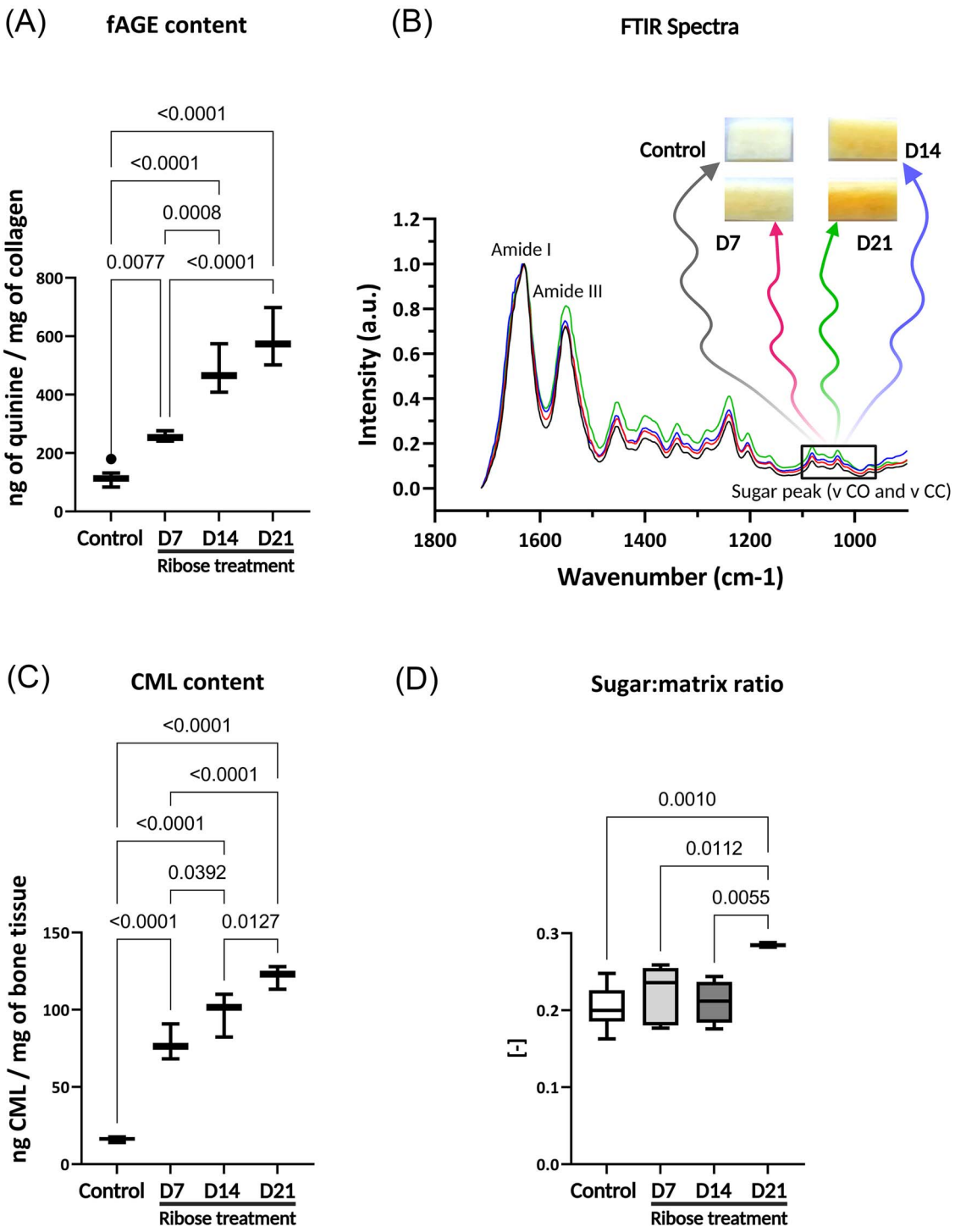

Figure 2. Higher fluorescent (fAGEs) and non-fluorescent (CML) advanced glycation end-products content in glycated bone samples. (A) Total fAGE content was significantly increased with 7, 14, and 21 incubation days compared to controls. (B) CML content significantly elevated with 7, 14, and 21 incubation days compared to control. (C) Specimen's FTIR spectrum. (D) The sugar-to-matrix ratio measured with FTIR spectroscopy was elevated at 21 incubation days compared to the control, 7-, and 14-d incubation times. Data is shown as box plots indicating median, lower quartiles, upper quartiles, and max and min values. Data was analyzed using ANOVA with the Tukey post hoc test. Abbreviations: fAGE, fluorescent advanced glycation end-products; CML, carboxymethyl-lysine; FTIR, Fourier transform infrared.

interstitial bone area remained similar across the groups; however, the hardness was significantly lower at 7-d ribose treatment compared to the control, and followed by an increase at 21-d ribose treatment to control levels (1.02 ± 0.06 GPa for the control vs 0.89 ± 0.11 GPa for the 7-d ribose treatment, $p = .011$; 1.03 ± 0.07 GPa for the 21-d vs 7-d, $p = .044$), as shown in Figure 4J-K.

J-integral (control vs 7-d ribose treatment, control vs 14-d ribose treatment, control vs 21-d ribose treatment) against crack length, *a*, was plotted with a 95% confidence interval of

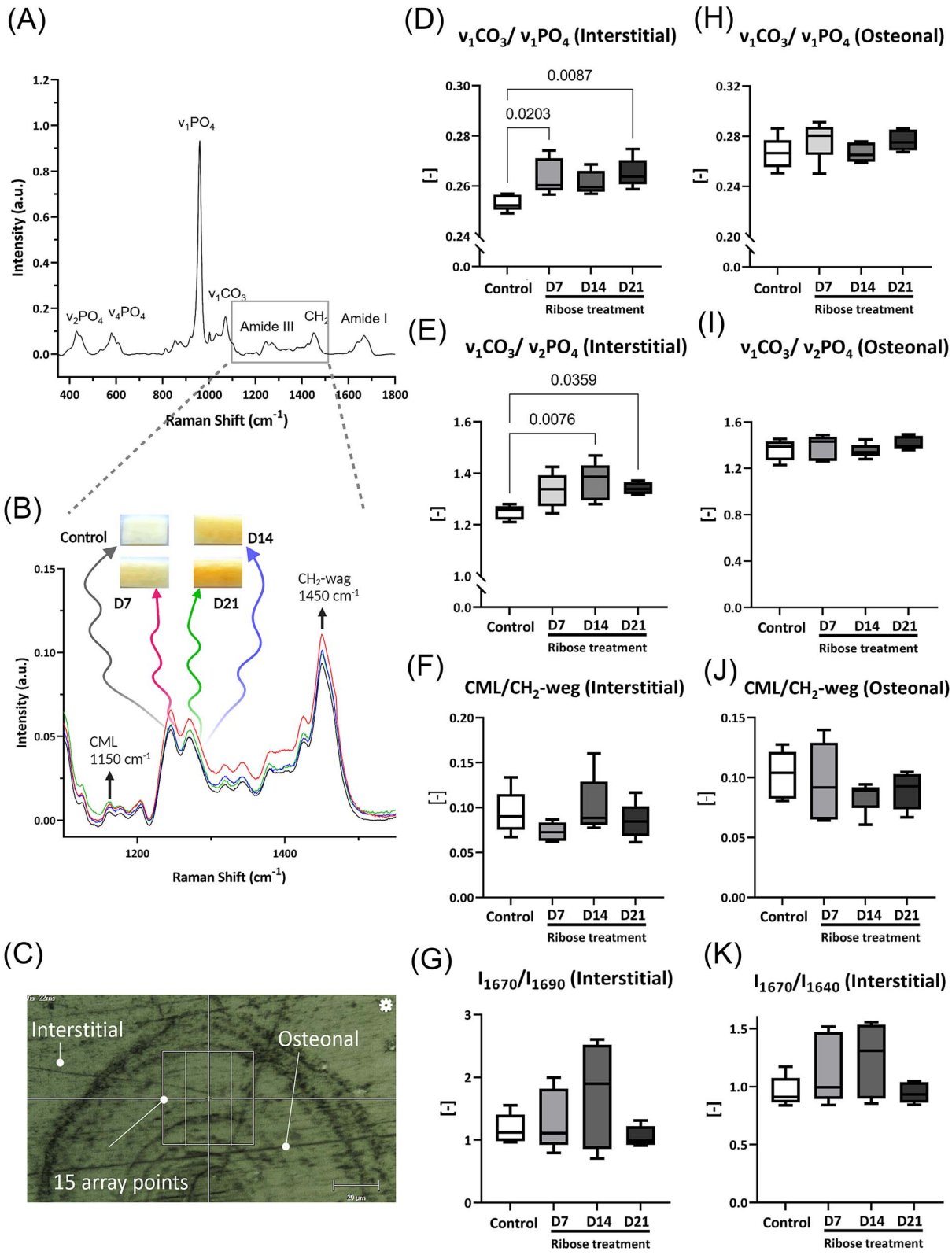

Figure 3. Altered carbonate-v1 and v2 phosphate ratios in interstitial bone matrix of glycated cortical bone. (A) Exemplary Raman spectrum. (B) CML peak and CH_2-wag peak in a bone sample. (C) 15 data points were measured in two areas (osteonal and interstitial). (D) The carbonate-to-v_1 phosphate ratio in the interstitial area was significantly higher after 7-, 21-d ribose treatment compared to the control group. (E) Carbonate-to-v_2 phosphate ratio in the interstitial area was significantly higher after 14- and 21-d ribose treatment compared to the control group. (F) CML/CH_2-wag ratio in interstitial area, (G) I_{1670}/I_{1690} ratio in interstitial area, (H-J) in osteonal area (H) carbonate-to-v_1 phosphate ratio, (I) carbonate-to-v_2 phosphate ratio, (J) CML/CH_2-wag ratio, and (K) I_{1670}/I_{1640} in interstitial area, are similar between the groups. Data are shown as box plots indicating median, lower quartiles, upper quartiles, and max and min values. Data were analyzed using ANOVA with the Tukey post hoc test. Abbreviation: CML, carboxymethyl-lysine.

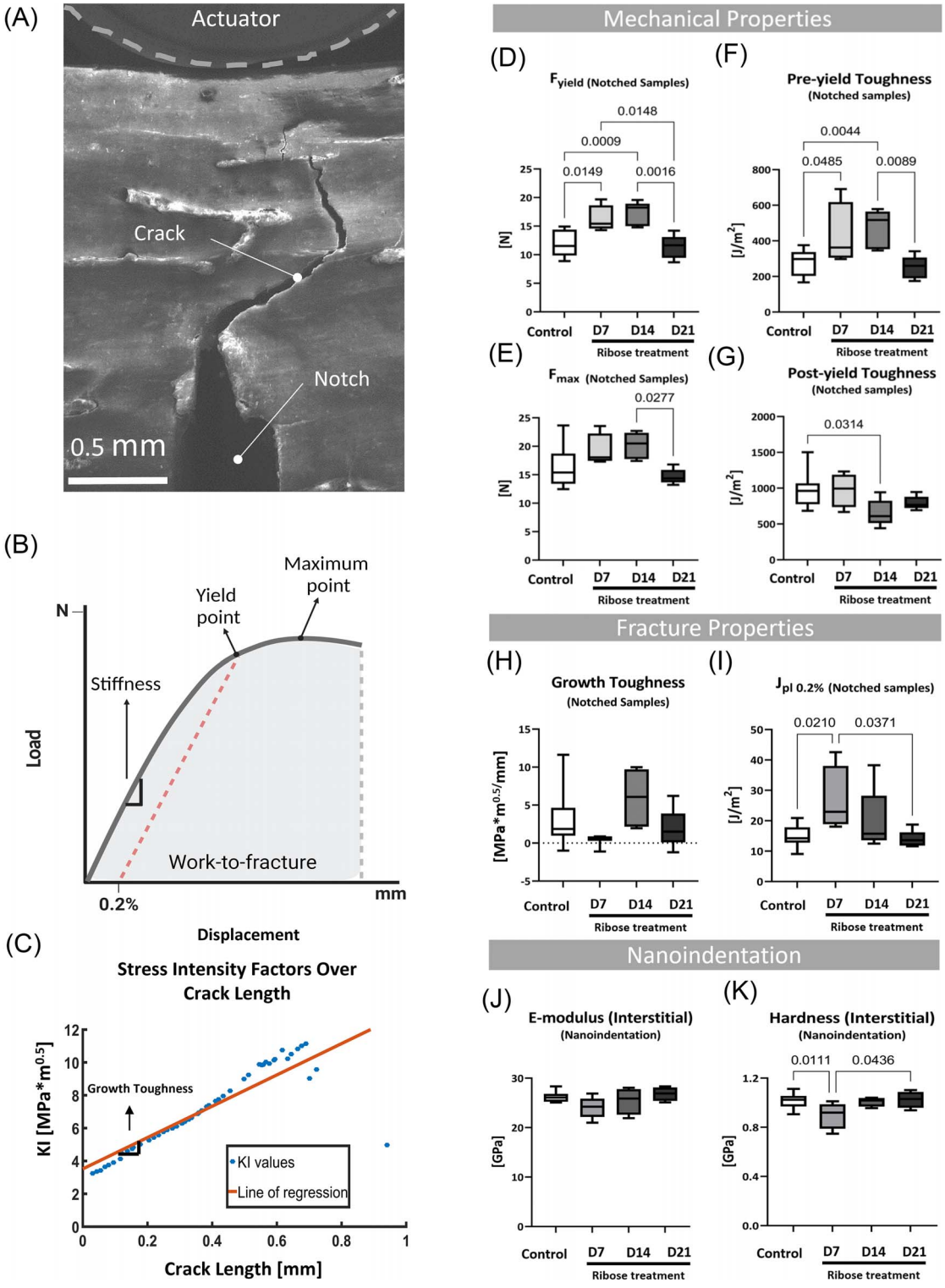

Figure 4. Glycation-dependent alterations of mechanical properties in notched bone samples. (A) Crack propagation was monitored with *in situ* SEM during a 3-point bending test of notched bone samples. (B) Illustration of load–displacement curve acquired during 3-point bending tests. (C) Example of the crack-resistance curve. (D) Force at yield point measured in notched samples was significantly higher after 7- and 14-d ribose treatment compared to controls and 21-d ribose treatment groups. (E) Maximum force measured during 3-point bending of notches bone samples elevated at 14-d ribose treatment and decreased at 21-d ribose treatment. (F) Toughness before bone yielding determined in notched bone samples showed significantly higher pre-yield toughness after 14-d ribose treatment compared to control and 21-d ribose treatment groups. (G) Toughness after bone yielding determined in notched bone samples showed significantly lower post-yield toughness after 14-d ribose treatment compared to the control. (H) Growth toughness was determined based on crack-resistance curve slopes from 3-point bending tests of notched samples and crack imaging with SEM; there were two image data losses in the 7-d treatment group due to technical issues. (I) J_{pl} at yield point ($J_{pl0.2\%}$) in notched bone samples showed significantly higher after 7-d ribose treatment compared to control and 21-d ribose treatment groups. (J) Elastic modulus measured from nanoindentation test showed no significant differences. (K) Hardness measured from the nanoindentation test displayed at 7-d ribose treatment was lower than the controls and the 21-d ribose treatment. Data are shown as box plots indicating the median, lower quartiles, upper quartiles, max, and min values. Data was analyzed using ANOVA with the Tukey post hoc test.

Table 3. Mechanical properties were similar in un-notched bone samples (all control samples were combined into one control group ($n = 15$) to compare to each glycation group ($n = 5$)).

	Control	D7	D14	D21
F_{max} [N]	116.20 ± 10.42	108.60 ± 4.22	117.90 ± 15.67	114.50 ± 14.26
F_{yield} [N]	98.36 ± 8.87	89.79 ± 5.32	100.20 ± 8.98	95.93 ± 4.86
Pre-yield toughness [J/m^2]	4149 ± 763.1	3281 ± 605.1	4102 ± 736.7	3768 ± 472.5
E-modulus [Gpa]	28.12 ± 4.79	31.64 ± 3.90	30.31 ± 0.88	28.85 ± 4.47
Post-yield displacement [mm]	0.10 ± 0.04	0.10 ± 0.03	0.09 ± 0.04	0.12 ± 0.07

Data are shown as mean ± SD. Data were analyzed using the ANOVA test with the Tukey post hoc test. F_{max} $p = .573$, .992, .991 for control vs D7, control vs D14, and control vs D21, respectively; $p = .576$, .846, .964 for D7 vs D14, D7 vs D21, and D14 vs D21, respectively. F_{yield} $p = .182$, .968, .933 for control vs D7, control vs D14, and control vs D21, respectively; $p = .185$, .618, .826 for D7 vs D14, D7 vs D21, and D14 vs D21, respectively. Pre-yield toughness $p = .100$, .999, .718 for control vs D7, control vs D14, and control vs D21, respectively; $p = .271$, .692, .873 for D7 vs D14, D7 vs D21, and D14 vs D21, respectively. *E*-modulus $p = .389$, .750, .987 for control vs D7, control vs D14, and control vs D21, respectively; $p = .958$, .724, .947 for D7 vs D14, D7 vs D21, and D14 vs D21, respectively. Post-yield displacement $p > .999$, .960, .870 for control vs D7, control vs D14, and control vs D21, respectively; $p = .978$, .924, .737 for D7 vs D14, D7 vs D21, and D14 vs D21, respectively. D7, 7-d ribose treatment; D14, 14-d ribose treatment; D21, 21-d ribose treatment.

Table 4. Micro-scale mechanical properties assessed using nanoindentation revealed that the *E* modulus was similar between control and ribose treatment groups in both interstitial and osteonal bone regions. However, hardness in the 7-d ribose treatment group was lower than in the control and the 21-d ribose treatment groups in interstitial regions. All control samples were combined into one control group ($n = 15$) for comparison with each glycation group ($n = 5$).

		Control	D7	D14	D21
Osteonal	*E* modulus [GPa]	23.64 ± 2.66	24.5 ± 1.86	23.5 ± 3.39	25.71 ± 2.68
	Hardness [GPa]	0.91 ± 0.0042	0.94 ± 0.00063	0.92 ± 0.0021	0.97 ± 0.0079
Interstitial	*E* modulus [GPa]	26.21 ± 1.06	24.06 ± 4.67	25.43 ± 7.44	26.83 ± 2.028
	Hardness [GPa]	1.02 ± 0.0036[a]	0.89 ± 0.0112[a,b]	1.01 ± 0.0014	1.03 ± 0.0046[b]

Data are shown as mean ± SD. Data were analyzed using ANOVA with the Tukey post hoc test. Osteonal region *E* modulus $p = .769$, .536, >.999 for control vs D7, control vs D14, and control vs D21, respectively; $p = .988$, .845, .667 for D7 vs D14, D7 vs D21, and D14 vs D21, respectively; hardness $p = .940$, .990, .399 for control vs D7, control vs D14, and control vs D21, respectively; $p = .997$, .886, .779 for D7 vs D14, D7 vs D21, and D14 vs D21, respectively. Interstitial region *E* modulus $p = .080$, .832, .909 for control vs D7, control vs D14, and control vs D21, respectively; $p = .599$, .081, .626 for D7 vs D14, D7 vs D21, and D14 vs D21, respectively; hardness $p = .011$, .994, .998 for control vs D7, control vs D14, and control vs D21, respectively; $p = .094$, .044, .984 for D7 vs D14, D7 vs D21, and D14 vs D21, respectively. D7, 7-d ribose treatment; D14, 14-d ribose treatment; D21, 21-d ribose-treatment. [a]Significant difference control vs R7, $p = .011$. [b]Significant difference R21 vs R7, $p = .044$.

second polynomial order (Figure 5A-C). The ribose treatment groups' fitting curves were lower than the control's, but no significant difference was found between the groups (Figure 5D).

Significant correlations between glycation status and mechanical and compositional properties

At the beginning of glycation (7-d and 14-d incubation), linear relationships were indicated between fAGE and F_{yield} and post-yield toughness; between CML and nanoscale hardness and elastic modulus, F_{max}, F_{yield}, pre-and post-yield toughness; between the carbonate-to-phosphate ν_1 ratio and F_{yield} and pre-yield toughness; and between the carbonate-to-phosphate ν_2 ratio and F_{max}, F_{yield} and pre- and post-yield toughness (see Table 5, column Control+D7+D14). At the end of glycation (21-d incubation), correlations were observed between fAGE and F_{yield}, pre-yield toughness, and *J* plastic at yield point ($J_{pl0.2\%}$), as well as between the carbonate-to-phosphate ratios and F_{yield} (see Table 5, column Control+D21).

Discussion

The study investigated the impact of glycation duration on mechanical, material, and compositional properties of human tibial cortical bone. *In vitro* glycation was conducted for 7, 14, and 21 d to induce varying concentrations of AGE accumulation in the bone matrix. Over time, fAGEs and CML measured from mass spectrometry increased, with a notably higher sugar-to-matrix ratio (glycation content in bone matrix) and carbonate-to-phosphate ratios after ribose incubation. Mechanical testing revealed an initial higher value in yield force and pre-yield toughness in notched specimens after 7 and 14 d of glycation, followed by a decline at 21 d to the control level. Nanoindentation testing on hardness at the interstitial region displayed an observable lower value at 7 d of glycation and then returned to the control level at 21 d. Correlations between compositional and mechanical properties were observed (Table 5). These findings demonstrate a complex connection between glycation duration and mechanical behavior. Bone is composed of a mineralized matrix primarily consisting of carbonated hydroxyapatite, ie, carbonate ions substituted into the crystal lattice. In the *in vitro* glycation process, where glycation is artificially induced in a laboratory setting, we observed that the carbonate-to-ν_1 and ν_2 phosphate ratios tend to be higher in samples glycated for 7, 14, and 21 d compared to controls. It is important to note that this ratio does not provide information regarding absolute changes in content but indicates a relative change. A higher ratio could indicate a reduction in phosphate content or an elevation in carbonate content within the mineral. While the possibility of phosphate dissolution within the bone matrix during the glycation process cannot be excluded because the phosphate contents in the ribose solutions were not measured before and after the process, it is unlikely that AGE accumulation would significantly affect either the phosphate content or mineral component carbonate within the bone matrix, but further investigation is necessary to validate this assumption.

Mechanical testing showed that the fracture mechanics of notched samples were affected by the glycation time, as indicated by higher pre-yield toughness at 7 d and 14 d of glycation, followed by lower levels at 21 d, returning to control

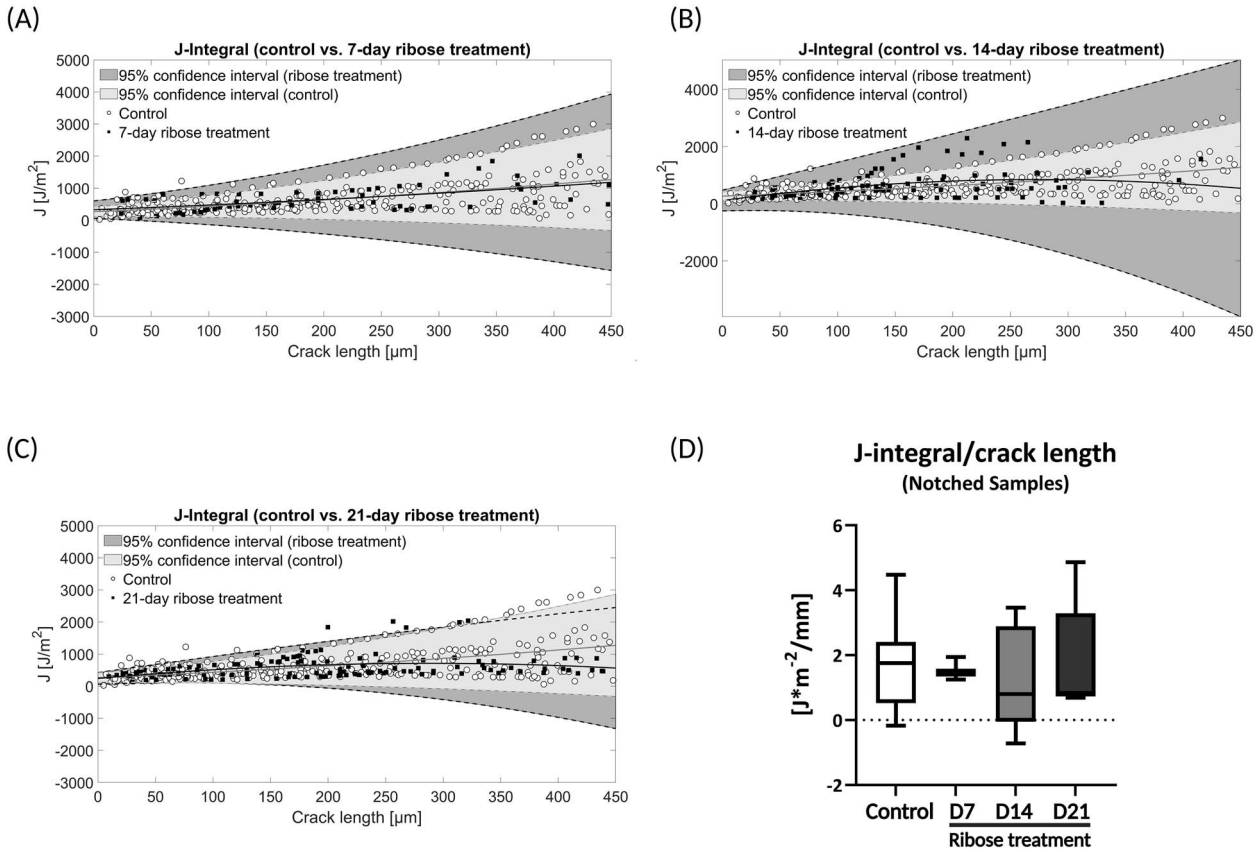

Figure 5. Similar *J*-integral among the control and ribose treatment groups. *J*-integral (A) control vs 7-d ribose treatment, (B) control vs 14-d ribose treatment, (C) control vs 21-d ribose treatment against crack length, a, was plotted with a 95% confidence interval of second polynomial order. The fitting curves in the ribose treatment groups were lower compared to the control, but (D) no significant difference was found between the groups. Data are shown as box plots indicating the median, lower quartiles, upper quartiles, max, and min values. Data was analyzed using ANOVA with the Tukey post hoc test.

Table 5. Correlations between compositional and mechanical properties.

	Control + D7+D14					Control + D21				
	fAGE	Sugar: matrix	CML	ν_1CO_3/ν_1PO_4	ν_1CO_3/ν_2PO_4	fAGE	Sugar: matrix	CML	ν_1CO_3/ν_1PO_4	ν_1CO_3/ν_2PO_4
H **(nanoindentation)**	−0.226	0.042	**−0.571**[a]	−0.487	−0.172	−0.012	0.235	0.297	−0.238	−0.041
E **(nanoindentation)**	−0.469	−0.067	**−0.741**[b]	−0.496	−0.397	0.136	−0.169	0.283	0.230	0.356
F_{max}	0.301	−0.001	**0.633**[a]	0.467	**0.614**[a]	−0.489	−0.540	−0.343	−0.055	0.011
F_{yield}	**0.561**[a]	0.097	**0.770**[b]	**0.547**[a]	**0.652**[a]	**−0.725**[a]	−0.444	−0.369	**0.018**[a]	**−0.024**[b]
Toughness (pre-yield)	0.467	0.309	**0.729**[b]	**0.591**[a]	**0.592**[a]	**−0.740**[b]	−0.323	−0.299	0.090	−0.047
Toughness (post-yield)	**−0.670**[b]	−0.134	**−0.586**[a]	−0.140	**−0.609**[a]	−0.306	0.074	−0.263	−0.687	−0.869
Toughness (total)	−0.424	−0.050	0.109	0.206	−0.119	−0.458	−0.157	−0.075	−0.354	−0.503
Growth toughness	0.228	0.000	−0.046	−0.262	−0.039	−0.013	−0.209	−0.201	−0.454	−0.333
K_{init0}	0.066	0.075	0.271	0.431	−0.066	0.263	0.044	0.056	0.262	0.203
$J_{el0.2\%}$	−0.173	−0.260	0.238	0.389	−0.108	−0.056	−0.291	−0.003	0.202	0.165
$J_{pl0.2\%}$	0.216	0.230	0.341	0.156	0.082	**−0.627**[a]	0.006	−0.296	−0.274	−0.064
$J_{total0.2\%}$	−0.011	0.095	0.249	0.405	−0.084	0.211	0.010	−0.015	0.189	0.161

Data were analyzed using Pearson correlation, and *r*-values are reported. The significant correlation is shown in bold. In the earlier stage of incubation (D7 and D14), correlations were observed between fAGE and F_{yield} and post-yield toughness; between CML and nanoscale hardness and elastic modulus, F_{max}, F_{yield}, pre- and post-yield toughness; between the carbonate-to-phosphate ν_1 ratio and F_{yield} and pre-yield toughness; and between the carbonate-to-phosphate ν_2 ratio and F_{max}, F_{yield} and pre- and post-yield toughness. At the end of glycation (D21), correlations were observed between fAGE and F_{yield}, pre-yield toughness, and *J* plastic at yield point ($J_{pl0.2\%}$), as well as between the carbonate-to-phosphate ratios and F_{yield}. D7, incubation after 7 d ribose treatment; D14, incubation after 14 d ribose treatment; D21, incubation after 21 d ribose treatment. [a]Significantly correlated $.01 < p < .05$, [b]$p < .01$.

levels. This transition from seemingly improved mechanical behavior at 7-14 d of glycation to impaired mechanical behavior at 21 d was unexpected. The results may suggest that the bone's resistance to yield and fracture was affected in opposite ways with increasing levels of AGE accumulation, underscoring a dynamic relationship between glycation duration

and mechanical properties. Furthermore, when comparing control, 7 and 14 d of incubation to 21 d, we found a positive correlation between compositional and mechanical properties in the earlier stage of incubation, which disappeared after 21 d of incubation (Table 5); instead, F_{yield} and pre-yield toughness were found to be negatively correlated with the fAGE level. This observation explains our results showing lower values in these parameters at 21 d of incubation, returning to control levels. Our study found a non-linear relationship between compositional and mechanical properties, indicating that before reaching a "saturation" of AGE accumulation, the level of glycation may not impair bone mechanical integrity but might even improve it. Further research could investigate the minimum incubation duration required to observe the effect of AGE accumulation on bone mechanical properties.

On the other hand, our investigation on un-notched bone samples did not show significant differences in mechanical properties between the groups. This observation suggests that the impact of AGE accumulation on bone mechanical properties may be less evident in specific conditions, particularly when the cortical porosity and cortical tissue mineral density remain unaltered and the mineralized bone matrix remains unaffected. However, when the bone tissue exhibits macro-scale alterations, characterized by pronounced structural irregularities, such as a notch, leading to elevated stress concentration in the notch area, a higher concentration of AGEs within the bone tissue could potentially contribute to enhancing the bone's resistance against yielding. Consequently, the mechanical indices derived from un-notched samples using an *in vitro* glycation model suggest that the influence of ribose-induced AGE accumulation in cortical bone with preserved bone structural units might not be the primary factor contributing to bone fragility, necessitating further investigation on other types of AGE. Following the investigation of notched bone samples, previous *in vitro* glycation studies on bovine cortical bone showed impaired bone mechanical properties in terms of yield stress, maximum strength,[16,19] fracture toughness, and J_{el}[16] with higher total fAGE content of 800%[16] and 1578%[19] in glycation groups compared to controls. However, another study using human cortical bone found no significant differences in fracture toughness, in combination with 126% higher fAGE accumulation in the glycation group compared to controls.[22] This quantitative data of fAGE accumulation further strengthens and reinforces our finding that an increased concentration of glycation (sugar/matrix) or elevated levels of AGEs (fAGEs) in the bone matrix indeed reduce the energy required to initiate and propagate cracks, ultimately resulting in a detrimental impact on mechanical properties and bone fragility.

Fracture toughness in bone is governed by two main contributors.[4] First, intrinsic toughness mechanisms enhance the ductility of the mineralized tissue, thereby impeding initial damage and hindering the growth of cracks. Second, extrinsic toughness mechanisms primarily function to arrest the propagation of cracks.[41] In our study, although there was no statistically significant difference in fracture toughness (assessed as stress intensity factor) between the groups, the growth toughness provided valuable insights into crack growth behavior and extrinsic toughness. A rising growth toughness was observed, indicating stable crack growth during fracturing. A steeper slope signifies a smaller crack length and greater stress intensity during crack propagation, implying higher extrinsic toughness. Conversely, a flatter slope indicates faster crack propagation and lower extrinsic toughness. Interestingly, our study demonstrated that after 7 d of glycation, the growth toughness was reduced compared to the control group; however, at 14 d of glycation, the growth toughness was higher by 60% compared to 7 d of glycation. Although this increase was not statistically significant, it suggests that AGE accumulation after 14 d of glycation may enhance the capacity for plastic deformation, thereby promoting elevated growth toughness. Another *in vitro* glycation study on the human cancellous bone[42] found that the growth toughness was significantly lower in a ribose treatment group compared to the control group when the total fAGEs were 103% higher compared to their control group.[42] Although there were no significant differences in overall fracture toughness between the groups in both studies, these findings provided interesting insights suggesting that fAGEs may have the potential to alter the behavior of mineralized collagen in terms of elastic stretching and their ability to absorb further deformation through inelastic mechanisms. These mechanisms could include intra/interfibrillar sliding, breaking/reforming of sacrificial bonds, and even the opening of dilatational bands at the mineral/collagen interface.[5–7]

The presented study has several limitations. The *in vitro* glycation models, including the use of 0.6 M ribose, do not directly reflect true clinical conditions.[43] However, despite these limitations, conducting the experiments in a controlled laboratory environment, with samples of similar tissue biological/biochemical age, as well as the pre-existing post-translational modifications, represents a significant source of information with a chance to assess the impact of AGE accumulation on bone fragility.

The purpose of ribose incubation in this study was not to directly mimic glycemic changes observed in clinical settings but to investigate the biomechanical properties of bone as AGEs accumulate with increasing incubation time. The biomechanical performance of our samples indicated that incubation time influenced the energy required to transition from elastic to plastic deformation.

The 3-point bending tests were conducted either in a vacuum chamber with a low pressure of 30 Pa or in an air environment, without continuous hydration as in the human body (ie, a hydration chamber during measurements). For the *in situ* SEM testing, although the samples were well-hydrated prior to testing, some dehydration likely occurred during testing in the vacuum chamber. Previous studies have demonstrated the influence of dehydration on bone material properties, including reduced toughness and initial crack resistance in an SEM environment compared to air.[28,44,45] However, another study found that these environmental conditions do not affect bone's elastic modulus because samples dry slowly from the surface and pores (eg, Haversian and Volkmann's canals, canaliculi, and lacunae) but retain bound water during the testing process.[46] Despite being unable to control the hydration status during testing, as it was not conducted in a hydration chamber, all samples were treated identically to facilitate comparison within the study. When comparing our results with others, the lower toughness parameters observed could be attributed to dehydration inside the vacuum chamber.

Besides, when considering the mechanical properties, the calculation of toughness relies on the specimens' dimensions and geometry,[29] and it is thus inadvisable to directly compare data on work to fracture from different investigators and studies.[47] There is still no universal standard for testing small

biological specimens for fracture behavior. Consequently, comparing our results with those from other studies using different methods and standards becomes challenging.

Raman spectroscopy was performed on dehydrated and fixed bone tissue It is acknowledged that dehydration and chemical treatment during embedding can potentially affect protein conformation, particularly that of collagen.[48] However, ethanol-fixed bone with MMA embedding did not significantly affect type B carbonation. Another study showed that the collagen-related 1660/1690 cm^{-1} ratio was lower in formaldehyde-fixed bone specimens compared to non-fixed bone specimens; the carbonate-to-phosphate ratio remained unaffected.[33] Despite these potential influences, all specimens underwent identical treatment, facilitating reliable group comparisons within this study.

Our study did not include non-incubated controls. Some studies have reported that incubation affects bone material properties.[18,49] However, we aimed to utilize the established method of *in vitro* ribose incubation to determine the role of AGEs induced by the treatment on the mechanical properties of bone rather than to study the effect of the incubation itself, as this has been investigated previously. Therefore, the non-ribose incubated control was sufficient for our study's purpose.

Despite our study design focusing on one individual body donor and generation of 90 test specimens, this deliberate choice was made to mitigate interindividual variability within heterogeneous cohorts. Including only one donor with sample extraction from one skeletal site enables us to uphold rigorous control over experimental conditions and sample geometry. The results yield valuable insights into the potential influence of ribose treatment duration on fracture mechanics. While the study was designed to minimize donor-specific effects, it is also important to acknowledge that individual donor characteristics, such as age, may have influenced the observed effects of *in vitro* glycation. This consideration should be considered when interpreting the study's implications.

Lastly, our study was designed to explore the mechanical behavior of bone under different durations of glycation. The sample size was influenced by the constraints of conducting an extensive multiscale analysis within a controlled environment. By minimizing confounding factors, such as gender, age, and bone site effects, we sought to maintain a high degree of experimental control and ensure the validity of our observations. Furthermore, since the *in vitro* glycation model amplified the accumulation of AGEs, we expected to discover significant differences in multiscale analysis even with a relatively small sample size. Similar sample sizes have been used in previous studies, such as Zimmerman et al.[11]

In summary, we successfully induced elevated accumulation of AGE in human cortical bone tissue by employing distinct glycation durations of 7, 14, and 21 d. Our observations demonstrated a progressive increase in fAGE/CML levels with extended incubation time. Regarding mechanical properties, notable distinctions emerged in the load–displacement curve of notched samples, revealing elevated pre-yield toughness and yield force at 14-d glycation compared to the control group, followed by a decline after 21 d of glycation to the control level. Additionally, a recent cohort study conducted in Sweden[50] reported an elevated fracture risk among individuals with type 2 diabetes presenting with a specific risk profile, including longer diabetes mellitus duration (≥15 yr). Considering this finding, it would be beneficial to expand the glycation protocol by incorporating longer incubation periods and additional time points, allowing for a more comprehensive assessment of the relationship between glycation, diabetes duration, and fracture risk.

In conclusion, our study illuminates the behavior of mechanical properties associated with varying glycation periods, underscoring the dynamic connection between glycation duration and mechanical characteristics. Furthermore, this study suggests that the accumulation of advanced glycation end-products may initially enhance the bone's ability to resist yielding. However, the accumulation starts to impair mechanical properties beyond a certain threshold. Although our study did not observe a harmful impact on bone mechanical properties and fragility at the levels tested, it implied that exceeding this threshold could lead to such adverse effects; further research is needed to fully understand the implications of prolonged AGE accumulation on bone fragility.

Acknowledgments

The authors thank Sandra Perkovic, Olga Winter, Michael Hahn, Timur Alexander Yorgan, Julius Fröhlich, Ali Hemany, Lukas Harms, Benjamin Bartsch, and Eric Grisolia Seifert (Department of Osteology and Biomechanics, University Medical Center Hamburg-Eppendorf) for their excellent technical and scientific support. Figures 1 and 4B were created with the help of BioRender.com.

Author contributions

Mei-Chun Lin (Conceptualization, Formal analysis, Investigation, Visualization, Writing—original draft, Writing— review & editing), Praveer Sihota (Conceptualization, Data curation, Formal analysis, Investigation, Software, Supervision, Validation, Visualization, Writing—original draft, Writing—review & editing), Sofie Dragoun Kolibová (Data curation, Investigation, Methodology, Resources), Imke A.K. Fiedler (Data curation, Formal analysis, Investigation, Methodology, Resources, Supervision, Writing—original draft, Writing—review & editing), Johannes Krug (Data curation, Investigation, Methodology, Resources, Software, Validation, Visualization, Writing—original draft, Writing—review & editing), Eva M. Wölfel (Conceptualization, Formal analysis, Investigation, Supervision, Validation, Writing—original draft, Writing—review & editing), Manuela Moritz (Data curation, Formal analysis), Maria Riedner (Data curation, Formal analysis), Benjamin Ondruschka (Resources), Mustafa Citak (Resources), Felix Klebig (Resources), Felix N. von Brackel (Investigation, Methodology, Resources), Mahan Qwamizadeh (Conceptualization, Formal analysis, Resources, Supervision, Validation), Katharina Jähn-Rickert (Conceptualization, Funding acquisition, Investigation, Methodology, Supervision, Writing—original draft, Writing—review & editing), and Björn Busse (Conceptualization, Funding acquisition, Investigation, Methodology, Project administration, Resources, Supervision, Writing—original draft, Writing—review & editing)

Supplementary material

Supplementary material is available at *JBMR Plus* online.

Funding

This project was funded by the European Union's Horizon 2020 Research and Innovation Program under the Marie Skłodowska-Curie grant agreement No 860898.

Conflicts of interest

The authors have nothing to disclose.

Ethical statement

Ethical approval number WT037/15 was provided by the local institutional review board.

Data availability

The datasets generated and/or analyzed during the current study are not publicly available but can be made available on reasonable request to the corresponding author.

References

1. Schwartz AV, Sellmeyer DE, Ensrud KE, et al. Older women with diabetes have an increased risk of fracture: a prospective study. *J Clin Endocrinol Metab*. 2001;86(1):32–38. https://doi.org/10.1210/jcem.86.1.7139
2. Yamamoto M, Yamaguchi T, Sugimoto T. Increased fracture rate in patients with type 2 diabetes mellitus is independent of its bone mineral density. *Clin Calcium*. 2006;16(8):1308–1314.
3. Carnevale V, Romagnoli E, D'Erasmo L, D'Erasmo E. Bone damage in type 2 diabetes mellitus. *Nutr Metab Cardiovasc Dis*. 2014;24(11):1151–1157. https://doi.org/10.1016/j.numecd.2014.06.013
4. Zimmermann EA, Gludovatz B, Schaible E, Busse B, Ritchie RO. Fracture resistance of human cortical bone across multiple length-scales at physiological strain rates. *Biomaterials*. 2014;35(21):5472–5481. https://doi.org/10.1016/j.biomaterials.2014.03.066
5. Poundarik AA, Diab T, Sroga GE, et al. Dilatational band formation in bone. *Proc Natl Acad Sci USA*. 2012;109(47):19178–19183. https://doi.org/10.1073/pnas.1201513109
6. Buehler MJ. Molecular nanomechanics of nascent bone: fibrillar toughening by mineralization. *Nanotechnology*. 2007;18(29):295102. https://doi.org/10.1088/0957-4484/18/29/295102
7. Fantner GE, Hassenkam T, Kindt JH, et al. Sacrificial bonds and hidden length dissipate energy as mineralized fibrils separate during bone fracture. *Nat Mater*. 2005;4(8):612–616. https://doi.org/10.1038/nmat1428
8. Kamml J, Ke C-Y, Acevedo C, Kammer DS. The influence of AGEs and enzymatic cross-links on the mechanical properties of collagen fibrils. *J Mech Behav Biomed Mater*. 2023;143:105870. https://doi.org/10.1016/j.jmbbm.2023.105870
9. Rosenberg J-L, Woolley W, Elnunu I, Kamml J, Kammer D-S, Acevedo C. Effect of non-enzymatic glycation on collagen nanoscale mechanisms in diabetic and age-related bone fragility. *Biocell*. 2023;47(7):1651–1659. https://doi.org/10.32604/biocell.2023.028014
10. Sihota P, Yadav RN, Dhaliwal R, et al. Investigation of mechanical, material, and compositional determinants of human trabecular bone quality in type 2 diabetes. *J Clin Endocrinol Metab*. 2021;106(5):e2271–e2289. https://doi.org/10.1210/clinem/dgab027
11. Zimmermann EA, Schaible E, Bale H, et al. Age-related changes in the plasticity and toughness of human cortical bone at multiple length scales. *Proc Natl Acad Sci USA*. 2011;108(35):14416–14421. https://doi.org/10.1073/pnas.1107966108
12. Damrath JG, Creecy A, Wallace JM, Moe SM. The impact of advanced glycation end products on bone properties in chronic kidney disease. *Curr Opin Nephrol Hypertens*. 2021;30(4):411–417. https://doi.org/10.1097/MNH.0000000000000713
13. Wölfel EM, Schmidt FN, Vom Scheidt A, et al. Dimorphic mechanisms of fragility in diabetes mellitus: the role of reduced collagen fibril deformation. *J Bone Miner Res*. 2022;37(11):2259–2276. https://doi.org/10.1002/jbmr.4706
14. Karim L, Moulton J, Van Vliet M, et al. Bone microarchitecture, biomechanical properties, and advanced glycation end-products in the proximal femur of adults with type 2 diabetes. *Bone*. 2018;114:32–39. https://doi.org/10.1016/j.bone.2018.05.030
15. Hunt HB, Torres AM, Palomino PM, et al. Altered tissue composition, microarchitecture, and mechanical performance in cancellous bone from men with type 2 diabetes mellitus. *J Bone Miner Res*. 2019;34(7):1191–1206. https://doi.org/10.1002/jbmr.3711
16. Britton M, Parle E, Vaughan TJ. An investigation on the effects of in vitro induced advanced glycation end-products on cortical bone fracture mechanics at fall-related loading rates. *J Mech Behav Biomed Mater*. 2023;138:105619. https://doi.org/10.1016/j.jmbbm.2022.105619
17. Jia S, Gong H, Cen H, et al. Influence of non-enzymatic glycation on the mechanical properties of cortical bone. *J Mech Behav Biomed Mater*. 2021;119:104553. https://doi.org/10.1016/j.jmbbm.2021.104553
18. Viguet-Carrin S, Farlay D, Bala Y, Munoz F, Bouxsein ML, Delmas PD. An in vitro model to test the contribution of advanced glycation end products to bone biomechanical properties. *Bone*. 2008;42(1):139–149. https://doi.org/10.1016/j.bone.2007.08.046
19. Vashishth D, Gibson GJ, Khoury JI, Schaffler MB, Kimura J, Fyhrie DP. Influence of nonenzymatic glycation on biomechanical properties of cortical bone. *Bone*. 2001;28(2):195–201. https://doi.org/10.1016/S8756-3282(00)00434-8
20. Merlo K, Aaronson J, Vaidya R, Rezaee T, Chalivendra V, Karim L. In vitro-induced high sugar environments deteriorate human cortical bone elastic modulus and fracture toughness. *J Orthop Res*. 2020;38(5):972–983. https://doi.org/10.1002/jor.24543
21. Vaidya R, Rezaee T, Edwards T, et al. Accumulation of fluorescent advanced glycation end products and carboxymethyl-lysine in human cortical and trabecular bone. *Bone Rep*. 2022;17:101634. https://doi.org/10.1016/j.bonr.2022.101634
22. Unal M, Uppuganti S, Dapaah DY, et al. Effect of ribose incubation on physical, chemical, and mechanical properties of human cortical bone. *J Mech Behav Biomed Mater*. 2023;140:105731. https://doi.org/10.1016/j.jmbbm.2023.105731
23. Wang J, Yin B, Liu G, et al. Microhardness distribution of the tibial diaphysis and test site selection for reference point indentation technique. *Medicine (Baltimore)*. 2019;98(29):e16523. https://doi.org/10.1097/MD.0000000000016523
24. *ASTM E 1820—01 Standard Test Method for Measurement of Fracture Toughness*. USA: ASTM International, 2003.
25. Schmidt FN, Zimmermann EA, Campbell GM, et al. Assessment of collagen quality associated with non-enzymatic cross-links in human bone using Fourier-transform infrared imaging. *Bone*. 2017;97:243–251. https://doi.org/10.1016/j.bone.2017.01.015
26. Sroga GE, Siddula A, Vashishth D. Glycation of human cortical and cancellous bone captures differences in the formation of Maillard reaction products between glucose and ribose. *PLoS One*. 2015;10(2):e0117240. https://doi.org/10.1371/journal.pone.0117240
27. Sihota P, Yadav RN, Poleboina S, et al. Development of HFD-fed/low-dose STZ-treated female Sprague-Dawley rat model to investigate diabetic bone fragility at different organization levels. *JBMR Plus*. 2020;44(10):e10379. https://doi.org/10.1002/jbm4.10379
28. Nyman JS, Roy A, Shen X, Acuna RL, Tyler JH, Wang X. The influence of water removal on the strength and toughness of cortical bone. *J Biomech*. 2006;39(5):931–938. https://doi.org/10.1016/j.jbiomech.2005.01.012
29. Rogers LL, Moyle DD. Effect of specimen size on work-of-fracture measurements. *J Biomech*. 1988;21(11):919–926. https://doi.org/10.1016/0021-9290(88)90130-3
30. Fett T, Rizzi G, Bahr H-A, Bahr U, Pham V-B, Balke H. Analytical solutions for stress intensity factor, T-stress and weight function for the edge-cracked half-space. *Int J Fract*. 2007;146(3):189–195. https://doi.org/10.1007/s10704-007-9152-8

31. Fett T, Munz D, Munz D. *Stress Intensity Factors and Weight Functions*. Southampton, UK ; Boston, Mass. USA: Computational Mechanics Publications; 1997:385 illustrations p.
32. Unal M, Ahmed R, Mahadevan-Jansen A, Nyman JS. Compositional assessment of bone by Raman spectroscopy. *Analyst*. 2021;146(24):7464–7490.
33. Fiedler IAK, Casanova M, Keplinger T, Busse B, Muller R. Effect of short-term formaldehyde fixation on Raman spectral parameters of bone quality. *J Biomed Opt*. 2018;23(11):1–6. https://doi.org/10.1117/1.JBO.23.11.116504
34. Paschalis EP, Gamsjaeger S, Klaushofer K. Vibrational spectroscopic techniques to assess bone quality. *Osteoporos Int*. 2017;28(8):2275–2291. https://doi.org/10.1007/s00198-017-4019-y
35. Unal M, Jung H, Akkus O. Novel Raman spectroscopic biomarkers indicate that postyield damage denatures bone's collagen. *J Bone Miner Res*. 2016;31(5):1015–1025. https://doi.org/10.1002/jbmr.2768
36. Gamsjaeger S, Srivastava AK, Wergedal JE, et al. Altered bone material properties in HLA-B27 rats include reduced mineral to matrix ratio and altered collagen cross-links. *J Bone Miner Res*. 2014;29(11):2382–2391. https://doi.org/10.1002/jbmr.2268
37. Morris MD, Mandair GS. Raman assessment of bone quality. *Clin Orthop Relat Res*. 2011;469(8):2160–2169. https://doi.org/10.1007/s11999-010-1692-y
38. Wölfel EM, Fiedler IAK, Dragoun Kolibova S, et al. Human tibial cortical bone with high porosity in type 2 diabetes mellitus is accompanied by distinctive bone material properties. *Bone*. 2022;165:116546. https://doi.org/10.1016/j.bone.2022.116546
39. Oliver WC, Pharr GM. An improved technique for determining hardness and elastic-modulus using load and displacement sensing indentation experiments. *J Mater Res*. 1992;7(6):1564–1583. https://doi.org/10.1557/JMR.1992.1564
40. Eastoe JE. The amino acid composition of mammalian collagen and gelatin. *Biochem J*. 1955;61(4):589–600. https://doi.org/10.1042/bj0610589
41. Ritchie RO. Mechanisms of fatigue crack-propagation in metals, ceramics and composites - role of crack tip shielding. *Mat Sci Eng a-Struct*. 1988;103(1):15–28. https://doi.org/10.1016/0025-5416(88)90547-2
42. Poundarik AA, Wu PC, Evis Z, et al. A direct role of collagen glycation in bone fracture. *J Mech Behav Biomed Mater*. 2015;52:120–130. https://doi.org/10.1016/j.jmbbm.2015.08.012
43. Willett TL, Voziyan P, Nyman JS. Causative or associative: a critical review of the role of advanced glycation end-products in bone fragility. *Bone*. 2022;163:116485. https://doi.org/10.1016/j.bone.2022.116485
44. Shin M, Zhang M, Vom Scheidt A, et al. Impact of test environment on the fracture resistance of cortical bone. *J Mech Behav Biomed Mater*. 2022;129:105155. https://doi.org/10.1016/j.jmbbm.2022.105155
45. Granke M, Does MD, Nyman JS. The role of water compartments in the material properties of cortical bone. *Calcif Tissue Int*. 2015;97(3):292–307. https://doi.org/10.1007/s00223-015-9977-5
46. Jimenez-Palomar I, Shipov A, Shahar R, Barber AH. Influence of SEM vacuum on bone micromechanics using in situ AFM. *J Mech Behav Biomed Mater*. 2012;5(1):149–155. https://doi.org/10.1016/j.jmbbm.2011.08.018
47. Ritchie RO, Koester KJ, Ionova S, Yao W, Lane NE, Ager JW 3rd. Measurement of the toughness of bone: a tutorial with special reference to small animal studies. *Bone*. 2008;43(5):798–812. https://doi.org/10.1016/j.bone.2008.04.027
48. Yeni YN, Yerramshetty J, Akkus O, Pechey C, Les CM. Effect of fixation and embedding on Raman spectroscopic analysis of bone tissue. *Calcified Tissue Int*. 2006;78(6):363–371. https://doi.org/10.1007/s00223-005-0301-7
49. Willett TL, Sutty S, Gaspar A, Avery N, Grynpas M. In vitro non-enzymatic ribation reduces post-yield strain accommodation in cortical bone. *Bone*. 2013;52(2):611–622. https://doi.org/10.1016/j.bone.2012.11.014
50. Axelsson KF, Litsne H, Kousoula K, Franzen S, Eliasson B, Lorentzon M. Risk of fracture in adults with type 2 diabetes in Sweden: a national cohort study. *PLoS Med*. 2023;20(1):e1004172. https://doi.org/10.1371/journal.pmed.1004172

JBMR Plus, 2025, 9, ziae151
https://doi.org/10.1093/jbmrpl/ziae151
Research Article